Pressure-broadened atomic Li(2s-2p) line perturbed by ground neon atoms in the spectral wings and core

Sabri Bouchoucha[1,†], Kamel Alioua[2], and Moncef Bouledroua[3]

[1] *Physics Department, Badji Mokhtar University, B. P.* 12, *Annaba* 23000, *Algeria*

[2] *Laboratoire de Physique de la Matière et du Rayonnement, Chérif Messaidia University, B. P.* 1553, *Souk-Ahras* 41000, *Algeria*

[3] *Laboratoire de Physique des Rayonnements, Badji Mokhtar University, B. P.* 12, *Annaba* 23000, *Algeria*

(Received 20 February 2017; revised manuscript received 31 March 2017; published online 27 May 2017)

Full quantum calculations are performed to investigate the broadening profiles of the atomic lithium Li(2s-2p) resonance line induced by interactions with ground Ne $\left(2s^2 2p^6\right)$ perturbers in the spectral wings and core. The $X^2\Sigma^+$, $A^2\Pi$, and $B^2\Sigma^+$ potential-energy curves of the two first low lying LiNe molecular states, as well as the corresponding transition dipole moments, are determined with *ab initio* methods based on the SA-CASSCF-MRCI calculations. The emission and absorption coefficients in the wavelength range 550–800 nm and the line-core width and shift are investigated theoretically for temperatures ranging from 130 K to 3000 K. Their temperature dependence is analyzed, and the obtained results are compared with the previous experimental measurements and theoretical works.

Keywords: pressure broadening, emission and absorption coefficients, linewidth, lineshift

PACS: 32.80.–t, 31.50.Bc, 31.50.Df, 32.70.Jz **DOI:** 10.1088/1674-1056/26/7/073202

1. Introduction

Currently, the main properties of the brown-dwarf and extrasolar-planet atmospheres are mostly extracted from the resonance lines of the alkali-metal atoms broadened by collisions with rare-gas atoms.[1–4] Information on the temperatures, densities, albedos, and composition of such atmospheres is contained in their observed spectral profiles. The interpretations of these profiles are based on models of the line pressure broadening.[5–14] Detailed knowledge of the line profiles as a function of temperature can be obtained from semiclassical[5–7] and full quantum[8–14] calculations using accurate molecular potential-energy curves (PECs) and transition dipole moments (TDMs) for the alkali-rare gas systems. The temperature dependence of the broadened line shape can then be used as valuable diagnostics of the extrasolar objects.

There are various recent theoretical studies of the alkali lines broadened by rare gases. These studies have employed semiclassical[5–7] and quantum[8–14] theories over a limited temperature domain. There are also some laboratory measurements of the broadened alkali lines in the wings. Generally, in these experiments, the alkali vapor is maintained in a fluorescence cell containing a rare-gas buffer, and the temperature of the cell is varied while keeping the alkali density constant. The alkali atoms are excited to the ^{2}P states by a continue-wave dye laser tuned to an appropriate wavelength close to the D lines. The fluorescence intensities of the alkali resonance lines induced by the buffer-gas in the wings are measured as a function of the wavelength and cell temperature. Various technical methods are used, namely, the laser induced fluorescence,[15–17] the two-step laser excitation,[18] the Doppler free two-photon spectroscopy,[19] the combination of the scattering and laser-spectroscopic measures,[20] and the high resolution laser spectroscopy including rotational analysis.[21]

In the present particular case, the quantal computations of the LiNe emission spectra made by Mason,[22] based on PECs and TDMs computed by two different methods, namely, the model potential and pseudopotential, are in clear disagreement with the available experimental data measured at $T = 670$ K by Scheps *et al.*[15] and at $T = 130$ K, 300 K, and 670 K by Havey *et al.*[23]

In this paper, we perform full quantum-mechanical calculations of the far-wing emission and absorption coefficients and line-core width and shift of the Li(2p-2s) resonance spectral line. For these calculations, we have chosen to use the potential-energy curves and transition dipole moments of the LiNe quasimolecule generated with the *ab initio* methods, in which we adopt the state-averaged complete active space self consistent field (SA-CASSCF) with the multireference configuration interaction (MRCI) procedures. We present the results for temperatures lying between 130 K and 3000 K and compare the obtained emission profiles with those measured by Scheps *et al.*[15] and Havey *et al.*[23] We further present the linewidth and shift results and compare them with the available theoretical and experimental data.

†Corresponding author. E-mail: bsa_ur@yahoo.fr

2. Pressure broadening

In the assumption of low densities, one may consider only binary collisions between lithium atoms evolving in a bath made of ground Ne atom. The study of the interaction between the atomic species of the gas mixture in thermal equilibrium is then reduced to the one of the temporarily formed LiNe quasi-molecules. For a given mixture, the spectra of the optical transitions of the lithium resonance line are broadened due to elastic collisions of Li(2p-2s) with Ne. This broadening phenomenon is reflected by the appearance of satellite structures in the far wings, which is generally accompanied by the width and shift of the line core.

In the following subsections, we are specifically interested in the emission and absorption profiles in the wings and the calculation of the linewidth and lineshift of the Lorentzian profile in the core.

2.1. In the wings

2.1.1. Emission profile

The Li(2s) Ne and Li(2p) Ne quasi-molecular systems have three molecular low-lying states, namely, the ground state $X^2\Sigma^+$ and the excited states $A^2\Pi$ and $B^2\Sigma^+$. As will be shown below, both X and B states are dominantly repulsive whereas the A state exhibits a shallow well. In such a case, one may consider at a given temperature T the free-free (ff) transitions between the B→X and A→X states and the bound-free (bf) transitions between the A→X states.

The free-free reduced emission coefficients $k_{\rm r}^{\rm ff}(\nu)$ at a frequency ν, corresponding to the transitions from the excited (e) to ground (g) continuum levels, at temperature T are given by[24–26]

$$k_{\rm r}^{\rm ff}(\nu) = \frac{64\pi^4\nu^3}{3hc^3}\omega\left(\frac{h^2}{2\pi\mu k_{\rm B}T}\right)^{3/2} \times \int_0^\infty {\rm d}\varepsilon_{\rm e}\sum_J (2J+1)\left|\left\langle u_{\rm e}^{\varepsilon J}\left|D(R)\right|u_{\rm g}^{\varepsilon J}\right\rangle\right|^2 \times \exp\left(-\frac{\varepsilon_{\rm e}}{k_{\rm B}T}\right). \quad (1)$$

Moreover, the bound-free reduced emission coefficients $k_{\rm r}^{\rm bf}(\nu)$ derived for the transitions from a set of upper bound levels to all lower continuum levels are expressed by

$$k_{\rm r}^{\rm bf}(\nu) = \frac{64\pi^4\nu^3}{3hc^3}\omega\left(\frac{h^2}{2\pi\mu k_{\rm B}T}\right)^{3/2} \times \sum_{vJ}(2J+1)\left|\left\langle u_{\rm e}^{vJ}\left|D(R)\right|u_{\rm g}^{\varepsilon J}\right\rangle\right|^2 \times \exp\left(-\frac{\varepsilon_{\rm e}}{k_{\rm B}T}\right). \quad (2)$$

The symbols c and h have their usual meanings; $k_{\rm B}$ is Boltzmann's constant, and μ is the reduced mass of the interacting atoms. The integer numbers v and J are the vibrational and rotational quantum numbers, respectively. The transition energy is related to the energy levels of the upper $\varepsilon_{\rm e}$ and lower $\varepsilon_{\rm g}$ states by the relationship

$$h\nu = \varepsilon_{\rm e} - \varepsilon_{\rm g} + h\nu_0, \quad (3)$$

with ν_0 being the resonance line frequency. The transition probabilities corresponding to the $A^2\Pi$ and $B^2\Sigma^+$ states are $\omega = 2/3$ and $\omega = 1/3$, respectively. The function $D(R)$, which depends on the internuclear separation R, represents the transition dipole moments. It assures the allowed transitions between the molecular states. We adopt here the approximation $J_{\rm u} \simeq J_{\rm l} = J$ justified by the involvement of large values of the rotational quantum numbers J. Moreover, the wavefunctions $u(R)$, appearing in both Eqs. (1) and (2), are the solutions of the radial wave equation

$$\frac{{\rm d}^2u(R)}{{\rm d}R^2} + \frac{2\mu}{\hbar^2}\left[\varepsilon - V(R) - \frac{J(J+1)\hbar^2}{2\mu R^2}\right]u(R) = 0, \quad (4)$$

where $V(R)$ is the electronic potential energy of the LiNe system at hand and ε is the energy of the relative motion. Note that the free wavefunctions $u(R) = u^{\varepsilon J}(R)$ are energy-normalized, while the bound wavefunctions $u(R) = u^{vJ}(R)$ are space-normalized, and both ε and $V(R)$ are measured with respect to the respective dissociation limits.

2.1.2. Absorption profile

To diagnose the absorption profiles, one has to consider the free-free and free-bound transitions between the molecular states $A^2\Pi \leftarrow X^2\Sigma^+$ and the free-free $B^2\Sigma^+ \leftarrow X^2\Sigma^+$ transitions.

The free-free reduced absorption coefficients $\alpha_{\rm r}^{\rm ff}(\nu)$ at temperature T are given by[10,12]

$$\alpha_{\rm r}^{\rm ff}(\nu) = \frac{8\pi^3\nu}{3c}\omega\left(\frac{h^2}{2\pi\mu k_{\rm B}T}\right)^{3/2} \times \int_0^\infty {\rm d}\varepsilon_{\rm e}\sum_J (2J+1)\left|\left\langle u_{\rm e}^{\varepsilon J}\left|D(R)\right|u_{\rm g}^{\varepsilon J}\right\rangle\right|^2 \times \exp\left(-\frac{\varepsilon_{\rm g}}{k_{\rm B}T}\right), \quad (5)$$

and the free-bound reduced absorption coefficients $\alpha_{\rm r}^{\rm fb}(\nu)$ are expressed by

$$\alpha_{\rm r}^{\rm fb}(\nu) = \frac{8\pi^3\nu}{3c}\omega\left(\frac{h^2}{2\pi\mu k_{\rm B}T}\right)^{3/2} \times \sum_{vJ}(2J+1)\left|\left\langle u_{\rm e}^{vJ}\left|D(R)\right|u_{\rm g}^{\varepsilon J}\right\rangle\right|^2 \times \exp\left(-\frac{\varepsilon_{\rm g}}{k_{\rm B}T}\right). \quad (6)$$

2.2. In the line core

Within the impact approximation, the elastic collisional broadening in the line core has been studied quantum mechanically by Baranger[27] and, thereafter, by Szudy and Baylis[28] and Allard and Kielkopf.[29] According to the simplified Baranger model, the full width at half maximum w and the shift s of the line are both interrelated by the relationship[28]

$$\frac{w}{2}+\mathrm{i}s = n\left\langle \frac{\pi\hbar}{\mu k}\sum_{l=0}^{\infty}(2l+1)\left\{1-\exp\left[2\mathrm{i}(\eta_l^{\mathrm{e}}-\eta_l^{\mathrm{g}})\right]\right\}\right\rangle_{\mathrm{av}}, \quad (7)$$

where η_l^{e} and η_l^{g} are the elastic phase shifts corresponding to the upper and lower molecular states, respectively. They depend on the angular momentum l and wavenumber k, which is linked to the relative energy $E=(\hbar k)^2/2\mu$ of the colliding atoms. In the above expression, the symbol $\langle\ldots\rangle_{\mathrm{av}}$ means the average taken over a Maxwellian velocity distribution. It can easily be shown that both linewidth w and lineshift s depend on the number density n of the foreign Ne atoms and are usually expressed by their rates given by the integral forms in terms of the dimensionless ratio $x=E/k_{\mathrm{B}}T$[27,30]

$$\frac{w}{n} = +4\sqrt{\frac{k_{\mathrm{B}}T}{2\mu\pi}}\int_0^{\infty} x\sigma_w(x)\exp(-x)\,\mathrm{d}x, \quad (8)$$

$$\frac{s}{n} = -4\sqrt{\frac{k_{\mathrm{B}}T}{2\mu\pi}}\int_0^{\infty} x\sigma_s(x)\exp(-x)\,\mathrm{d}x, \quad (9)$$

where σ_w and σ_s are the linewidth and lineshift cross sections, respectively,

$$\sigma_w = \frac{4\pi}{k^2}\sum_{l=0}^{\infty}(2l+1)\sin^2\left(\eta_l^{\mathrm{e}}-\eta_l^{\mathrm{g}}\right), \quad (10)$$

$$\sigma_s = \frac{\pi}{k^2}\sum_{l=0}^{\infty}(2l+1)\sin\left[2\left(\eta_l^{\mathrm{e}}-\eta_l^{\mathrm{g}}\right)\right]. \quad (11)$$

The energy-dependent phase shifts $\eta_l=\eta_l(E)$ are obtained by solving the radial wave equation (4), with J being substituted by l and forcing the free wavefunctions $u(R)$ to behave asymptotically like

$$u(R)\sim\sin\left(kR-\frac{1}{2}l\pi+\eta_l\right). \quad (12)$$

In this case, the linewidth and lineshift cross sections $\sigma_{w,s}$ are evaluated as the weighted average cross sections

$$\sigma_{w,s}=\frac{1}{3}\sigma_{w,s}^{(\mathrm{B}-\mathrm{X})}+\frac{2}{3}\sigma_{w,s}^{(\mathrm{A}-\mathrm{X})}, \quad (13)$$

where $\sigma_{w,s}^{(\mathrm{B}-\mathrm{X})}$ and $\sigma_{w,s}^{(\mathrm{A}-\mathrm{X})}$ correspond to the allowed transitions $\mathrm{B}^2\Sigma^+$–$\mathrm{X}^2\Sigma^+$ and $\mathrm{A}^2\Pi$–$\mathrm{X}^2\Sigma^+$, respectively.

The line profiles in the wings and the Lorentzian profiles in the line core are significantly influenced by the electronic interaction potentials $V(R)$ and the transition dipole moments $D(R)$, which both should be carefully determined.

3. Potential-energy curves and transition dipole moments

The accuracy of the spectral profiles is strongly related to the quality of the LiNe potential-energy curves and transition dipole moments that will be determined below. When the Li atom, either in the ground (2s) ^{2}S or the first excited (2p) ^{2}P state, interacts with the ground Ne($2s^2 2p^6\ ^1$S) atom, they both approach each other along one of the molecular curves $\mathrm{X}^2\Sigma^+$, $A^2\Pi$, and $\mathrm{B}^2\Sigma^+$.

In order to determine the potential-energy curves involved in the LiNe interactions and the corresponding transition dipole moments $D_{\Sigma-\Sigma}(R)$ and $D_{\Pi-\Sigma}(R)$, we have performed MRCI calculations[31,32] using reference functions derived from the SA-CASSCF approach[33,34] and the Dunning augmented correlation consistent polarized core/valence quadrupole zeta (AUG-CC-PCVQZ) basis on the Li and Ne atoms.[35] Among the 13 electrons of the LiNe molecule, only two inner electrons from the Ne atom are frozen in the subsequent calculations, so 11 valence electrons are explicitly treated. The active space, at long range, contains the following orbitals: 5σ corresponding to $\mathrm{Li}(1\mathrm{s},2\mathrm{s},2\mathrm{p}_0)$, $\mathrm{Ne}(2\mathrm{s},2\mathrm{p}_0)$ and 4π corresponding to $\mathrm{Li}(2\mathrm{p}_{\pm})$, $\mathrm{Ne}(2\mathrm{p}_{\pm})$. These 9 active orbitals are distributed among irreducible representations a_1, b_1, b_2, and a_2 of the C_{2v} symmetry as follows: $6,2,2,0$. The Davidson correction is introduced to estimate the effect of the higher-order excitations.[36] The basis-set superposition error (BSSE) has also been corrected via the counterpoise procedure.[37] All the calculations are performed using the quantum-chemistry package MOLPRO.[38] The computations of the potential curves and dipole moments are performed over the interval 1 Å $\leqslant R \leqslant$ 21 Å.

The computed potential data points for the $\mathrm{X}^2\Sigma^+$, $\mathrm{A}^2\Pi$, and $\mathrm{B}^2\Sigma^+$ states are smoothly connected to the long-range form

$$V(R)\sim-\frac{C_6}{R^6}-\frac{C_8}{R^8}-\frac{C_{10}}{R^{10}} \quad (14)$$

beyond $R\geqslant 21$ Å. In the above equation, the constant parameters C_6, C_8, and C_{10} are the well-known dispersion coefficients. For the construction of the three X, A, and B states in their long-range regions, the adopted values of the dispersion coefficients C_n ($n=6$, 8, and 10) are those calculated by Mitroy and Zhang,[39] which are listed in Table 1. The generated PECs are shown in Fig. 1. According to these curves, one may notice that both X and B states are mostly repulsive, whereas the A state exhibits a very shallow well.

Table 1. Adopted dispersion coefficients into the LiNe potential constructions. All the data are given in atomic units.

Dispersion coefficients	Molecular states		
	$\mathrm{X}^2\Sigma^+$	$\mathrm{A}^2\Pi$	$\mathrm{B}^2\Sigma^+$
C_6	4.379×10^1	5.492×10^1	9.822×10^1
C_8	2.229	7.522×10^2	1.549×10^4
C_{10}	1.531×10^5	3.586×10^4	1.849×10^6

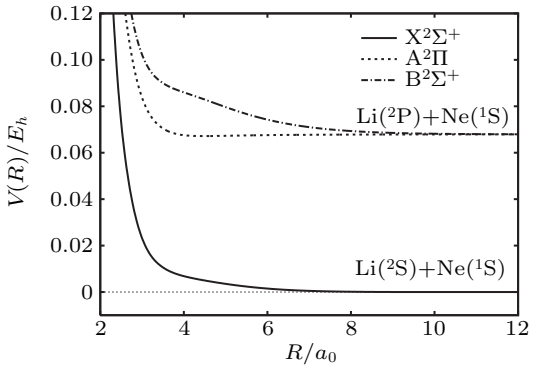

Fig. 1. The LiNe potentials $V(R)$ for the ground $X^2\Sigma^+$ and excited $A^2\Pi$ and $B^2\Sigma^+$ molecular states.

For the ground $X^2\Sigma^+$ state, we have found a well depth $D_e = 5.535$ cm^{-1} occurring at the equilibrium position $R_e = 5.398$ Å. From the measured absolute total scattering cross sections, Dehmer and Wharton[40] fitted the obtained X-state curve to the Buckingham–Corner $(6,8)$ potential and determined $D_e = 9.61 \pm 2.11$ cm^{-1} and $R_e = 4.979 \pm 0.217$ Å. However, using the extrapolated complete basis set limit, Kerkines and Mavridis[41] calculated the values $D_e = 7.68$ cm^{-1} and $R_e = 5.2$ Å. This indicates that the obtained values are acceptable.

For the first excited state $A^2\Pi$, we have determined a binding energy $D_e = 190.87$ cm^{-1} around the position $R_e = 2.328$ Å. Both data can be compared with the measured values $D_e = 212 \pm 5$ cm^{-1} and $R_e = 2.307 \pm 0.011$ Å of Lee and Havey[42] and $D_e = 225 \pm 30$ cm^{-1} and $R_e = 3.223$ Å of Balling *et al.*[17]

For the second excited molecular state $B^2\Sigma^+$, the potential parameters $D_e = 2.729$ cm^{-1} and $R_e = 7.303$ Å demonstrate that the potential is very shallow and the values are quantitatively closer to those obtained theoretically by Kerkines and Mavridis,[41] namely, $D_e = 3.7$ cm^{-1} and $R_e = 7.1$ Å. The corresponding data, $D_e = 3.2$ cm^{-1} and $R_e = 7.144$ Å, have also been determined by Czuchaj *et al.*[43] Furthermore, the calculations reveal that the molecular states $X^2\Sigma^+$, $A^2\Pi$, and $B^2\Sigma^+$ can hold 1, 6, and 1 bound vibrational levels, respectively. The rotationless vibrational energy levels are displayed in Table 2.

Table 2. Calculated rotationless vibrationnal energy levels $E(v, J = 0)$, in units of cm^{-1}, relative to the $X^2\Sigma^+$, $A^2\Pi$, and $B^2\Sigma^+$ LiNe quasimolecule.

v	$X^2\Sigma^+$	$A^2\Pi$	$B^2\Sigma^+$
0	−2.141	−144.617	−0.944
1		−79.660	
2		−38.897	
3		−14.748	
4		−3.303	
5		−0.097	

One can exploit these potential curves to predict the number of satellite structures and their positions on the spectra by adopting the classical rule that assumes satellites appear where the curves of the potential differences between the ground and excited states present extrema. The potential differences, converted to wavelengths, are plotted in Fig. 2 against the internuclear distance R. The difference $(V_A - V_X)$ exhibits a pronounced extremum around the wavelength 761 nm at the position near $3.41a_0$, whereas the difference $(V_B - V_X)$ shows another extremum close to the value 574 nm at the separation distance $3.6a_0$. From these differences, one may conclude that the potential short-range regions are expected to affect considerably the properties of the predicted satellites and reveal that the first and the second satellites originated from the A–X and B–X transitions in the red and blue wings, respectively.

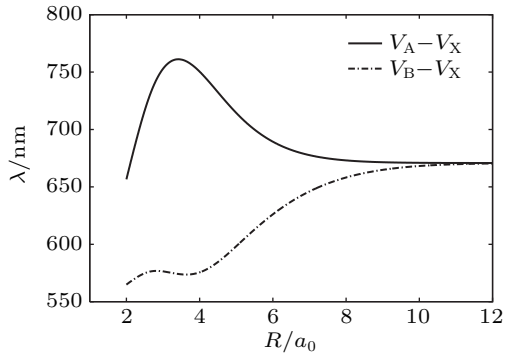

Fig. 2. The LiNe difference potentials in units of wavelengths as a function of the internuclear distance R.

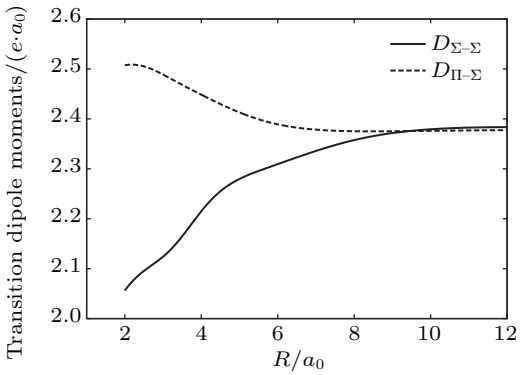

Fig. 3. Transition dipole moments $D_{\Sigma-\Sigma}(R)$ and $D_{\Pi-\Sigma}(R)$ as a function of the internuclear distance R.

On the other hand, the transition dipole moments $D_{\Sigma-\Sigma}(R)$ and $D_{\Pi-\Sigma}(R)$ are correlated to the transitions between the A and B excited states and the ground X state, respectively. They have been computed in this work by using the MRCI wavefunctions. In particular, as proposed by Chu and Dalgarno,[44] the transition dipole moments behave at large distances like

$$D(R) \sim D_\infty \left(1 + \gamma/R^3\right). \tag{15}$$

The calculated TDM at infinity is $D_\infty = 2.38$ a.u., and the constant γ appearing in formula (15) is equal to $-\delta(v_0)$ for

the Π–Σ transitions and $\gamma = +2\delta(\nu_0)$ for the Σ–Σ transitions, with $\delta(\nu_0) = 2.68a_0^3$ being the dynamic polarizability of the dominant gas Ne at the resonance frequency ν_0 of the alkali metal Li.[44] The constructed LiNe transition dipole moments are displayed in Fig. 3.

4. Results and discussion

The potential-energy curves and transition dipole moments correctly built in the preceding section can now be used in the computation of the emission and absorption profiles and the linewidth and lineshift of the Lorentzian line core profile.

4.1. Computational details

The calculation of the reduced emission and absorption coefficients, including all the bound and quasi-bound levels, is carried out for all temperatures with a frequency step size $\Delta\nu = 10$ cm^{-1}. The rotational quantum number J does not exceed the values 250 and 15 for the free-free and free-bound transitions, respectively. The mathematical integrals appearing in Eqs. (1) and (5) are evaluated with the Gauss–Laguerre quadrature in which 100 weighted points are used.[45] The radial wave equation (4) is solved numerically with the Numerov algorithm,[46] and the matrix elements are computed using the Simpson rule with equally spaced intervals $\Delta R = 0.01a_0$.

In addition, the possible values of the angular momentum l needed in the calculation of the cross sections, defined in Eqs. (10) and (11), vary from 0 to 1000. The very large values of the angular momentum l involved in these equations are treated semiclassically from some cutoff value l_c to be determined for each value of the colliding energy E. Consequently, the phase shifts can be approximated by[47]

$$\eta_l(k) \simeq -\frac{\mu}{\hbar^2}\int_{R_0}^{\infty}\frac{V(R)}{\sqrt{(kR)^2 - l^2}}R\mathrm{d}R, \tag{16}$$

with $R_0 \approx 1/k$. If the potential $V(R)$ is assumed to decrease rapidly in the field of large values of R, then the condition $V(R) \lll E$ is fulfilled in the interval of integration. For the LiNe molecule, the long-range potential is given by Eq. (14) for the ground and excited states, then the expression of the phase shift (16) is reduced to the sum of partial phase shifts

$$\eta_l \approx \eta_l^{(6)} + \eta_l^{(8)} + \eta_l^{(10)}, \tag{17}$$

with

$$\eta_l^{(n)}(k) \simeq +\frac{\mu C_n k^{n-2}}{\hbar^2 l^{n-1}} f(n), \tag{18}$$

where $f(6) = 3\pi/16$, $f(8) = 15\pi/96$, and $f(10) = 105\pi/768$.[47]

4.2. Emission profiles

The full quantum-mechanical LiNe emission profiles around the wavelength $\lambda_0 = 670.8$ nm result from the $A^2\Pi \rightarrow X^2\Sigma^+$ and $B^2\Sigma^+ \rightarrow X^2\Sigma^+$ transitions. Keeping in mind that the ground X and excited B molecular states are mostly repulsive, which is not the case of the excited A state, the most probable transitions are therefore of the free-free or bound-free type. The computed spectra, as displayed in Fig. 4, are particularly presented around the resonance line in the wavelength interval 550–800 nm at six different temperatures $T = 130$ K, 300 K, 670 K, 1000 K, 2000 K, and 3000 K. Moreover, the calculations show that the red side comes from the contributions of the free-free and bound-free $A^2\Pi \rightarrow X^2\Sigma^+$ transitions, while the blue side of the resonance line arises exclusively from the free-free $B^2\Sigma^+ \rightarrow X^2\Sigma^+$ transitions.

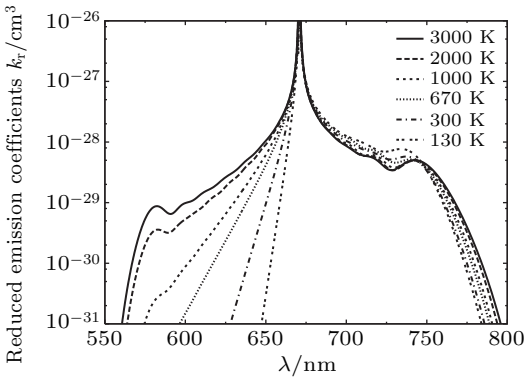

Fig. 4. The full quantum-mechanical reduced emission coefficients at different temperatures.

In building the red wings of the emission spectra, the calculations reveal that the bound-free contributions dominate the majority of the red wings at the lowest temperatures and decrease rapidly for higher wavelengths. On the other hand, the free-free contributions, though they complement the bound-free ones, dominate the red wings near the line center, but diminish quickly in importance as the wavelength increases. An immediate consequence of these considerations is that a significant increase of temperature generates the decrease of the relative importance due to bound-free and free-free contributions.

A detailed analysis of Fig. 4 shows that the wings of the LiNe emission spectra have a decreasing allure from the unperturbed resonance line and fall to the extreme values of the wavelengths. The spectra exhibit satellite structures in both sides of the resonance line. They show in particular undulations at higher temperatures, which disappear practically in the blue wings as the temperature decreases.

The red wings spectra exhibit a satellite around the wavelength 743 nm, which moves slowly at low temperatures towards the line center. On the other hand, a satellite arises in the blue side in the vicinity of the wavelength 581 nm, which vanishes at lower temperatures below $T = 670$ K.

The precision of the present calculations is checked by comparing the determined spectra at different temperatures with available experimental and theoretical results. Indeed, to the best of our knowledge, the only available experimental results of the LiNe emission profiles are those measured experimentally by Scheps *et al.*[15] and Havey *et al.*[23] Figure 5 compares their measured results with the present theoretical calculations. The spectra have also been obtained quantum mechanically by Mason[22] at the temperatures $T = 130$ K, 300 K, and 670 K using two distinct interatomic potentials based on model potential and pseudopotential methods. He compared his theoretical results with the experimental data at the same temperatures and noted clear discrepancies. One should point out that the measured profiles, given in arbitrary units by Scheps and Havey and their collaborators,[15,23] have been rescaled here in order to match as closely as possible with our calculated profiles. It is easy to see from Fig. 5 that the overall shapes of the calculated profiles are in reasonable agreement with the measurements for all temperatures, excluding a slight deviation in the near wing at $T = 130$ K.

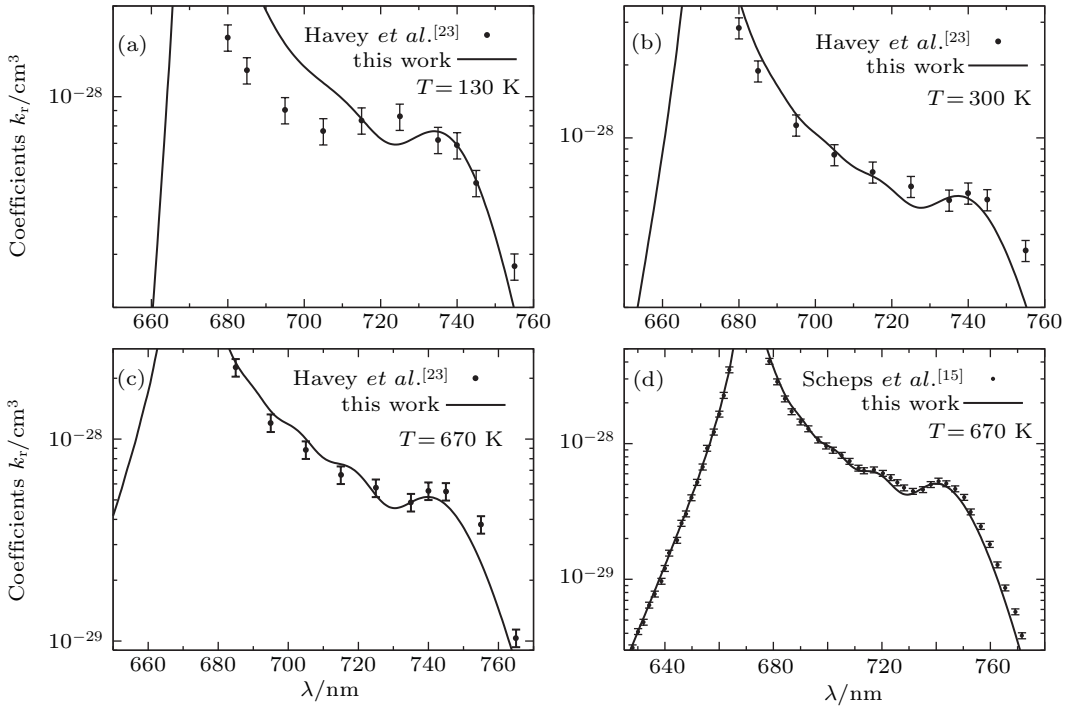

Fig. 5. Theoretical reduced emission coefficients computed at $T = 130$ K, 300 K, and 670 K. The present results are compared with those measured by Scheps *et al.*[15] and Havey *et al.*[23]

4.3. Absorption profiles

The LiNe absorption coefficients are resulting from the contributions of the free-free A←X and B←X, and free-bound A←X transitions. More precisely, the shape of the LiNe spectra is basically determined by the free-free B←X transitions in the blue wings and by the free-free and free-bound A←X transitions in the red wings. Furthermore, in the red wings, the free-free transitions are dominant compared to the free-bound ones for all considered temperatures. Hence, in contrast with the emission phenomena, the free-free transitions for all temperatures dominate the LiNe absorption spectra.

As for the reduced emission coefficients, we illustrate in Fig. 6 the LiNe reduced absorption coefficients at the same temperatures, i.e., $T = 130$–3000 K. A close inspection of this figure shows that the profiles decrease rapidly from the resonance line passing by a plateau to fall with a high slope in the limit of the wavelength range. The spectra present undulations that end with two satellites in both wings at higher temperatures, which disappear at lower temperatures. As one may see, the absorption profiles exhibit two satellite peaks beyond $T = 670$ K, one in the red wings close to 743 nm and the other in the blue wings around 581 nm. One may notice that the satellite positions in the absorption spectra are similar to those obtained with the emission profiles.

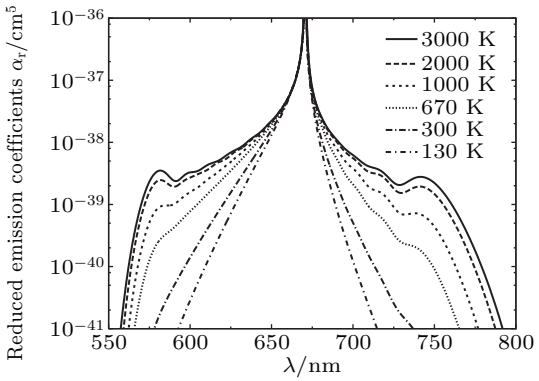

Fig. 6. The full quantum-mechanical reduced absorption coefficients at different temperatures.

4.4. Width and shift

For the calculation of the linewidth and the lineshift parameters related to the Li $(2p \rightarrow 2s)$ atomic line perturbed by foreign Ne atoms, the simplified model of Baranger may be utilized, since the used buffer-gas temperatures allow us to assume occurrence essentially of elastic collisions and to neglect the degeneracy of the atomic states due to spin–orbit effects. To determine the phase shifts needed in the calculation of the linewidth and lineshift cross sections, the energy interval from 10^{-11} to $10^{-1}E_h$ Hartree is chosen, and the range of the adopted angular momentum l is 0–1000. The computed linewidth and shift cross sections from Eqs. (10) and (11) are given respectively in Figs. 7 and 8, where the average curves are determined with Eq. (13).

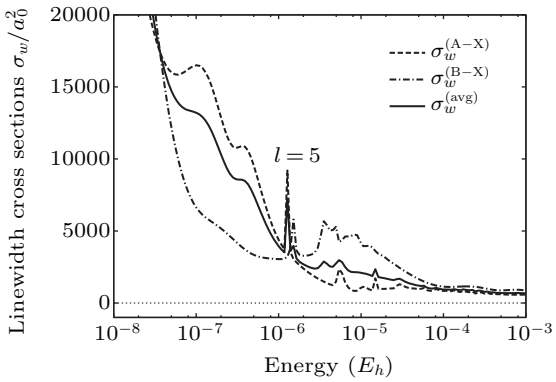

Fig. 7. Energy dependence of the linewidth cross sections for the A–X and B–X transitions and their weighted statistical average.

Figure 7 presents the curves of the linewidth cross sections in connection with the A–X and B–X transitions. The shapes of these curves have almost the same behavior. Between the two energy limits, the linewidth cross sections exhibit peaks arising from partial waves of order $l = 5$ and higher. Likewise, figure 8 displays the shapes of the lineshift cross sections for the A–X and B–X transitions. The curves demonstrate the same behavior and present higher values at low energies. After a sudden decrease, they oscillate among the resonance extrema and become very small at large energies.

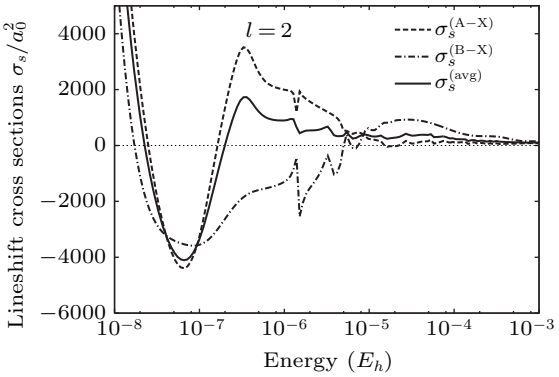

Fig. 8. Energy dependence of the lineshift cross sections for the A–X and B–X transitions and their weighted statistical average.

When evolving in a bath made of Ne atoms, the linewidth and lineshift rates, w/n and s/n, of the Li resonance line are calculated at a few temperatures, namely, $T = 400$ K, 500 K, 600 K, and 630 K. The obtained results are compared with those measured experimentally by Gallagher[48] and Harris *et al.*[49] and with those calculated by semiclassical methods by Kielkopf[50] and Lwin *et al.*[51] All the results are gathered in Table 3, which shows that the obtained linewidth rates are very close to the measured values in the limits of the experimental uncertainties. Discrepancies are shown for the lineshift at the temperatures $T = 400$ K, 600 K, and 630 K. Such discrepancies are probably due to the use of Baranger's simplified theoretical model, which is rather suitable for perturbers made of light atoms and radiators with non degenerate atomic levels.[27]

Table 3. Comparison of our calculated linewidth and lineshift rates with experimental measurements of Gallagher[48] and Harris *et al.*[49] with the previous theoretical calculations of Kielkopf[50] and Lwin *et al.*[51]

Temperature	$w/n/(10^{-20}\ \mathrm{cm^{-1}/cm^{-3}})$			$s/n/(10^{-20}\ \mathrm{cm^{-1}/cm^{-3}})$		
T/K	This work	Refs.		This work	Refs.	
400	0.76	0.76 ± 0.04	[48]	−0.90	-0.30 ± 0.06	[48]
		0.79	[50]		−0.46	[50]
500	0.83	0.85 ± 0.34	[48]	−0.93	-0.49 ± 0.32	[48]
600	0.89	0.80	[51]	−0.97	−0.10	[51]
630	0.90			−0.98	-0.22 ± 0.07	[49]

Table 4. Fitting coefficients that appear in Eq. (19) for temperature dependence of the linewidth and shift rates. They are given in units of $10^{-20}\ \mathrm{cm^{-1}/cm^{-3}}$.

Rates	a	b	c	d	e
w/n	+0.359	+1.179	−0.608	+0.204	−0.027
s/n	−0.752	−0.332	−0.058	−0.006	+0.004

In order to find out the variation law of the linewidth and lineshift rates as a function of temperature T, we have determined these rates in the temperature range $130\ \mathrm{K} \leq T \leq 3000$ K. The computed results of the rates demonstrate that they fit correctly the polynomial law of the form

$$\left.\begin{matrix} \dfrac{w}{n} \\ \dfrac{s}{n} \end{matrix}\right\} = a + b\widehat{T} + c\widehat{T}^2 + \mathrm{d}\widehat{T}^3 + e\widehat{T}^4, \tag{19}$$

where $\widehat{T} = T/1000$. The fitting coefficients are gathered together in Table 4. The dependence of the w/n and s/n rates on temperature and their corresponding fitting curves are shown in Fig. 9. As a final note, the temperature dependence seems to vary in a decidedly systematic way.

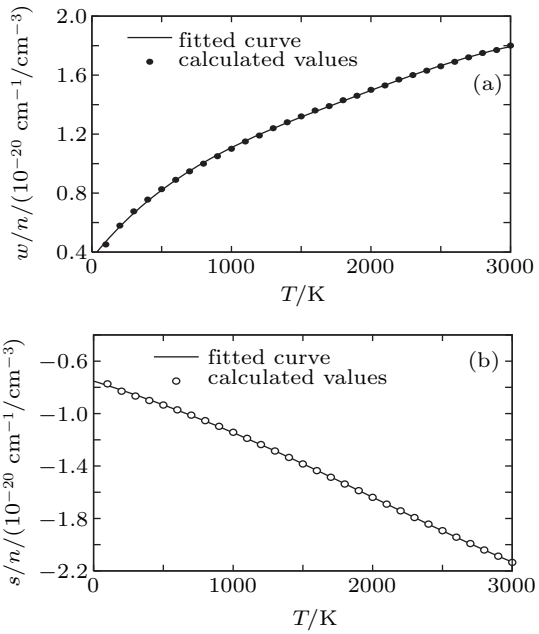

Fig. 9. Temperature dependence of (a) the linewidth rate w/n and (b) the lineshift rate s/n. The full lines represent the numerical fitting function (19).

5. Conclusion

Full quantum-mechanical calculations of the LiNe emission and absorption profiles have been performed in the wavelength range 550–800 nm, and their variations with temperature from 130 K to 3000 K have been examined. Within the Baranger impact approximation, the linewidth and shift have also been determined in the temperature interval 130 K $\leq T \leq$ 3000 K. Accurate LiNe ground $X^2\Sigma^+$ and excited $A^2\Pi$ and $B^2\Sigma^+$ interatomic potentials and transition dipole moments have been primarily computed with MOLPRO using the *ab initio* SA-CASSCF/MRCI methods, including the Davidson and BSSE corrections. As a result, both emission and absorption spectra show a blue satellite around the wavelength 581 nm, for $T \approx$ 1000–3000 K, and a red satellite near the wavelength 743 nm, for $T \approx$ 130–3000 K, in the emission spectra, and for $T \approx$ 1000–3000 K, in the absorption spectra. The emission coefficients and the linewidth and shift data show good agreements with the experiments.

References

[1] Burrows A 2005 *Nature* **433** 261
[2] Sharp C M and Burrows A 2007 *ApJS* **168** 140
[3] Burgasser A J, Cushing M C, Kirkpatrick J D, *et al.* 2011 *ApJ* **735** 116
[4] Leggett S K, Saumon D, Marley M S, *et al.* 2012 *ApJ* **748** 74
[5] Allard N F 2014 *Adv. Space Res.* **54** 1285
[6] Allard N F, Nakayama A, Stienkemeier F, Kielkopf J F, Guillon G and Viel A 2014 *Adv. Space Res.* **54** 1290
[7] Blank L and Weeks D E 2014 *Phys. Rev. A* **90** 022510
[8] Zhu C, Babb J F and Dalgarno A 2005 *Phys. Rev. A* **71** 052710
[9] Zhu C, Babb J F and Dalgarno A 2006 *Phys. Rev. A* **73** 012506
[10] Alioua K and Bouledroua M 2006 *Phys. Rev. A* **74** 032711
[11] Mullamphy D F T, Peach G, Venturi V, Whittingham I B and Gibson S G 2007 *J. Phys. B* **40** 1141
[12] Alioua K, Bouledroua M, Allouche A R and Aubert-Frécon M 2008 *J. Phys. B* **41** 175102
[13] Boutarfa H, Alioua K, Bouledroua M, Allouche A R and Aubert-Frécon M 2012 *Phys. Rev. A* **86** 052504
[14] Bouhadjar F, Alioua K, Bouazza M T and Bouledroua M 2014 *J. Phys. B* **47** 185201
[15] Scheps R, Ottinger C, York G and Gallagher A 1975 *J. Chem. Phy.* **63** 2581
[16] Havey M D, Frolking S E, Wright J J and Balling L C 1981 *Phys. Rev. A* **24** 3105
[17] Balling L C, Wright J J and Havey M D 1982 *Phys. Rev.* **26** 1426
[18] Behmenburg W, Kaiser A, Rebentrost F, Jungen M, Smith M, Luo M and Peach G 1998 *J. Phys. B* **31** 689
[19] Rosenberry M A and Stewart B 2011 *J. Phys. B* **44** 055207
[20] Grosser J, Hoffmann O, Rebentrost F and Tiemann E 2014 *J. Phys. B* **47** 165102
[21] Hager G D, Lott G E, Archibald A J, Blank L, Weeks D E and Perram G P 2014 *J. Quant. Spectrosc. Radiat. Transfer* **147** 261
[22] Mason C R 1991 (PhD. Thesis) (London: University College of London)
[23] Havey M D *Private Communication to Mason C R* [22]
[24] Herman P S and Sando K M 1978 *J. Chem. Phys.* **68** 1153
[25] Sando K M 1971 *Mol. Phys.* **21** 439
[26] Woerdman J P 1985 *J. Phys. B* **18** 4205
[27] Baranger M 1958 *Phys. Rev.* **111** 481
[28] Szudy J and Baylis W E 1975 *J. Quant. Spectrosc. Radiat. Transfer* **15** 641
[29] Allard N F and Kielkopf J F 1982 *Rev. Mod. Phys.* **54** 1103
[30] Reggami L, Bouledroua M, Allouche A R and Aubert-Frécon M 2009 *J. Quant. Spectrosc. Radiat. Transfer* **110** 72
[31] Werner H J and Knowles P J 1985 *J. Chem. Phys.* **82** 5053
[32] Knowles P J and Werner H J 1985 *Chem. Phys. Lett.* **115** 259
[33] Werner H J and Knowles P J 1988 *J. Chem. Phys.* **89** 5803
[34] Knowles P J and Werner H J 1988 *Chem. Phys. Lett.* **145** 514
[35] Woon D E and Dunning Jr T H 1994 *J. Chem. Phys.* **100** 2975
[36] Davidson E R and Silver D W 1977 *Chem. Phys. Lett.* **53** 403
[37] Boys S F and Bernardi F 1970 *Mol. Phys.* **19** 553
[38] Werner H J, Knowles P J and Lind R 2008 *Package of ab initio programs Molpro version* 2008.1
[39] Mitroy J and Zhang J Y 2007 *Phys. Rev. A* **76** 032706
[40] Dehmer P and Wharton L 1972 *J. Chem. Phys.* **57** 4821
[41] Kerkines I S K and Mavridis A 2001 *J. Phys. Chem. A* **105** 1983
[42] Lee C J and Havey M D 1991 *Phys. Rev. A* **43** 6066
[43] Czuchaj E, Rebentrost F, Stoll H and Preuss H 1989 *Chem. Phys.* **136** 79
[44] Chu X and Dalgarno A 2002 *Phys. Rev. A* **66** 024701
[45] Press W H , Flannery B P, Teukolsky S A and Vetterling W T 1987 *Numerical Recipes. The Art of Scientific Computing* (New York: Cambridge University Press)
[46] Numerov B 1933 *Publ. Observatoire Central Astrophys. Russ.* **2** 188
[47] Mott N F and Massey H S W 1965 *The Theory of Atomic Collisions* (Oxford: Oxford University Press)
[48] Gallagher A 1975 *Phys. Rev. A* **12** 133
[49] Harris M, Lwin N and McCartan D G 1982 *J. Phys. B* **15** L831
[50] Kielkopf J F 1976 *J. Phys. B* **9** L547
[51] Lwin N, McCartan D G and Lewis E L 1977 *ApJ* **213** 599